Electronic Supplementary Information

High K-storage performance based on the synergy of dipotassium terephthalate and ether-based electrolyte

Kaixiang Lei[a], Fujun Li[a,b]*, Chaonan Mu[a], Jianbin Wang[a], Qing Zhao[a], Chengcheng Chen[a] and Jun Chen[a,b]*

[a]Key Laboratory of Advanced Energy Materials Chemistry (Ministry of Education), College of Chemistry, Nankai University, Tianjin 300071, China
[b]Collaborative Innovation Center of Chemical Science and Engineering, Nankai University, Tianjin 300071, China

E-mail: fujunli@nankai.edu.cn; chenabc@nankai.edu.cn

Experimental Section

Material Synthesis: K_2TP was synthesized by refluxing. Briefly, 1.935 g of potassium hydroxide was dissolved in 40 mL of deionized water under stirring. Then, 1.73 g of terephthalic acid was added to the above solution at 50 °C, and absolute ethanol was added to precipitate the product at 90 °C. After refluxing for 12 h, the as-obtained precipitate was filtered with ethanol and vacuum-dried at 150 °C overnight.

Material Characterization: The as-synthesized K_2TP was characterized by power X-ray diffraction (XRD) on a Rigaku X-2500 diffractometer using Cu Kα radiation, scanning electron microscopy (SEM, JEOL JSM-7500F), and infrared spectroscopy (IR, BIORAD FTS 6000 FTIR). The thermal stability of K_2TP was estimated by TG-DSC analyzer (NETZSCH, STA 449 F3) at a heating rate of 5 °C min^{-1} from 25 to 800 °C in air. Besides, X-ray photoelectron spectroscopy (XPS, Perkin Elmer PHI

1600 ESCA system) was used to characterize the intermediates at different discharge and charge states.

Electrochemical Tests: CR2032 coin cells, which were assembled in an Ar-filled glove box (O_2 ≤5 ppm, H_2O ≤ 2 ppm), were used to investigate electrochemical performance of K_2TP. Before preparing the working electrode, K_2TP and super P (60:30) were ball-milled in a planetary ball mill at 300 rpm for 1 h to reduce the size of K_2TP and increase the contact between K_2TP and conductive carbon. Then, the above mixture was mixed with 10% polyvinylidene fluoride (PVdF) in N-methyl-2-pyrrolidone (NMP). The obtained slurry was pasted onto a Cu foil and then dried in a vacuum oven at 110 °C for 8 h. The mass loading of the active material is 1.2-1.6 mg cm^{-2}. The potassium metal was employed as counter electrode and reference electrode. Glassy-fiber filter was used as separator. The electrolyte was 1 M KPF_6 in 1, 2-dimethoxyethane (DME), 0.8 M KPF_6 in ethylene carbonate/diethyl carbonate (EC/DEC, v/v = 1:1), 1 M KPF_6 in ethylene carbonate/propylene carbonate (EC/PC, v/v = 1:1), and 1 M KPF_6 in PC, respectively. 40 μL of electrolyte was used in each coin cell. Galvanostatic charge/discharge tests were carried out on Land CT2001A battery instrument in the voltage range of 0.1−2 V (vs. K/K^+). The applied current densities are based on the mass of K_2TP. Cyclic voltammetry was tested with Parstat 263A electrochemical workstation (AMTECT Company) between 0.1 and 2 V. All the tests were performed at room temperature. The electrode was taken out from the cycled cell and then washed with DME to remove the residual electrolyte in an argon-filled glove box to conduct IR and XPS tests.

Computational Method: All the calculations were implemented by Gaussian 09 Software.[S1] The structure optimizations were relaxed at the B3LYP[S2,S3] level with the 6-31+G (d,p) basis set. The HOMO plots of K_2TP with two negative charge was visualized by Multiwfn.[S4]

Table S1. Refined structural parameters of K_2TP by the Rietveld method.[a]

atom	site	occ.	x	y	z
K1	4e	1	0.61022	0.20362	0.16110
O1	4e	1	0.35191	0.18530	0.16424
O2	4e	1	0.32623	0.30002	-0.03283
C1	4e	1	0.13570	0.39816	0.02578
C2	4e	1	0.07864	0.35423	0.11444
C6	4e	1	0.05476	0.54573	-0.08945
C7	4e	1	0.28199	0.28534	0.05386
H2A	4e	1	0.13110	0.25709	0.19183
H6A	4e	1	0.09123	0.57798	-0.15012

[a] Monoclinic, space group P21/c, a = 10.566, b = 3.950, c = 11.546, β = 113.04°, and V = 443.48 Å^3.

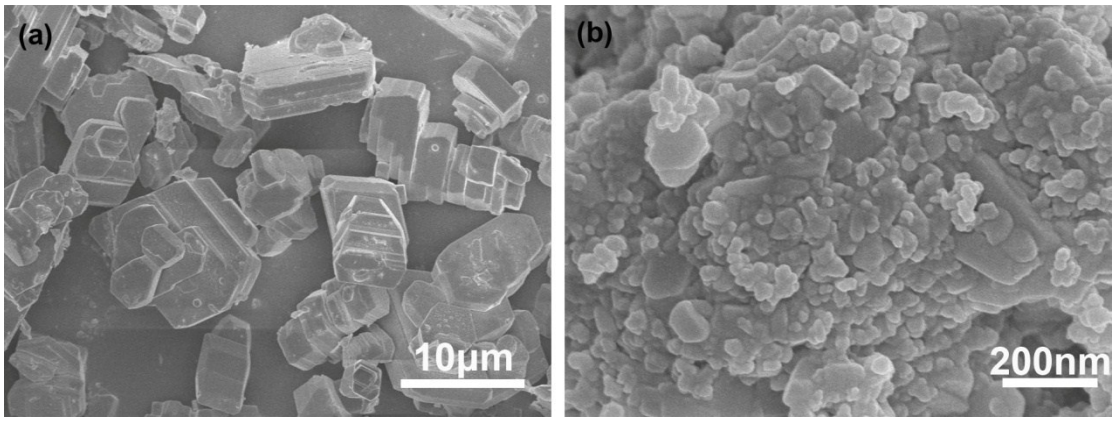

Fig. S1 SEM images of (a) K_2TP and (b) K_2TP/SP.

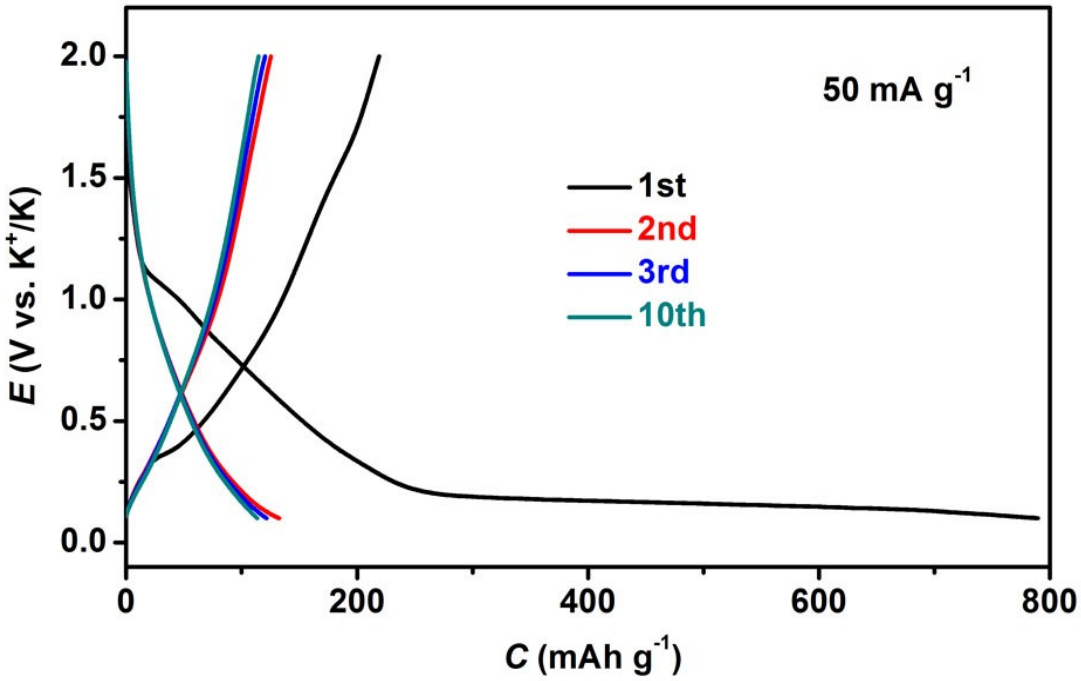

Fig. S2 Galvanostatic discharge/charge profiles of Super P at 50 mA g^{-1}.

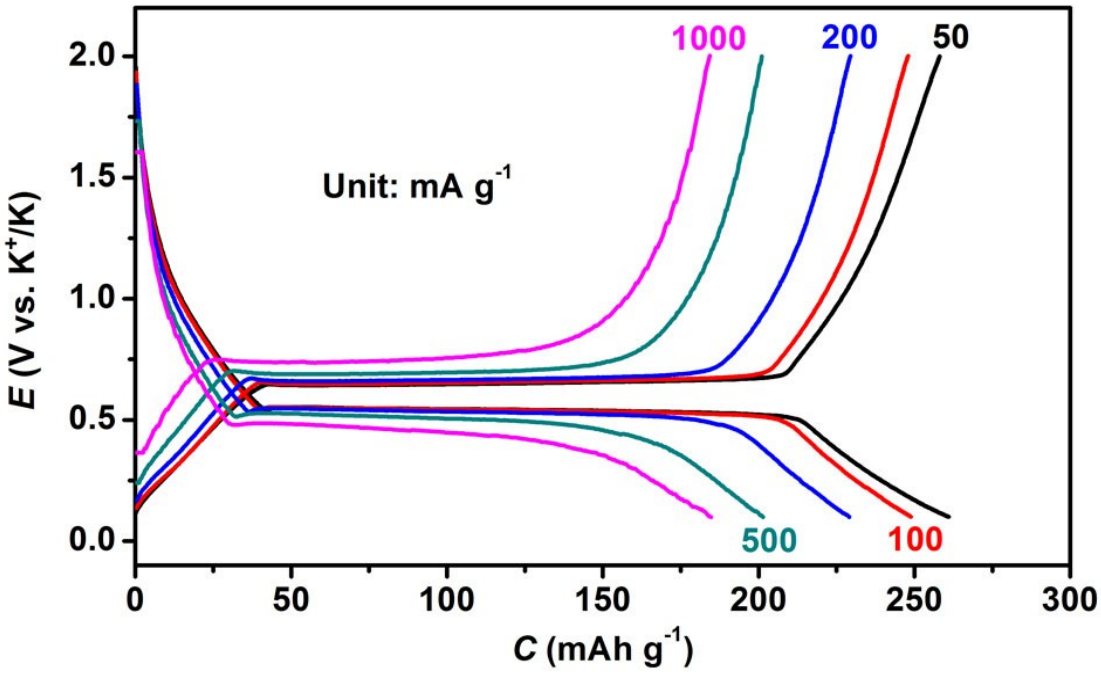

Fig. S3 Charge-discharge curves of K_2TP at different current densities.

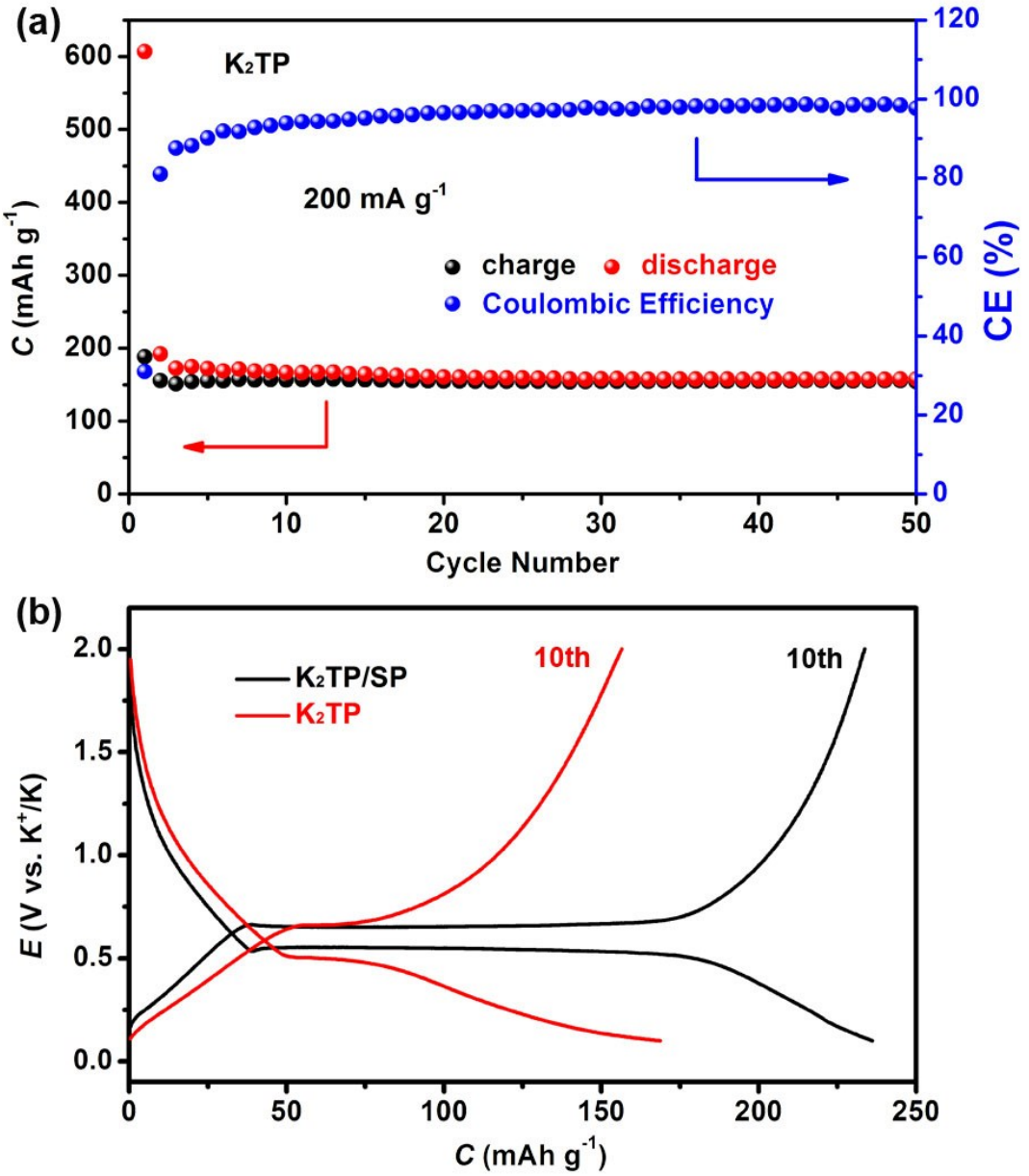

Fig. S4 (a) The cycle stability of bulk K_2TP and (b) the selected 10th charge-discharge curves of bulk K_2TP and K_2TP /SP at 200 mA g^{-1}.

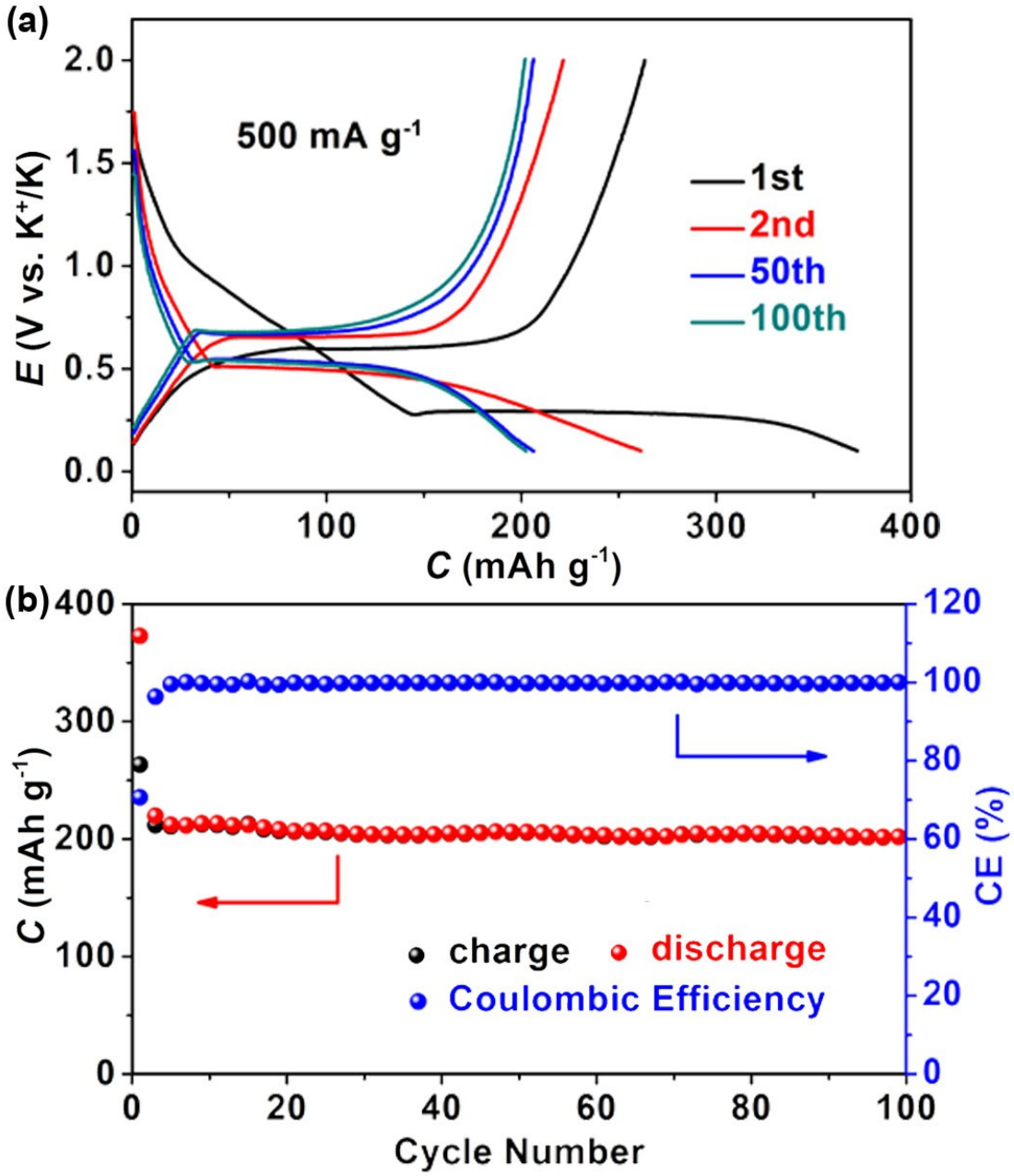

Fig. S5 (a) Charge-discharge curves of the selected cycles and (b) cycle stability at 500 mA g^{-1}.

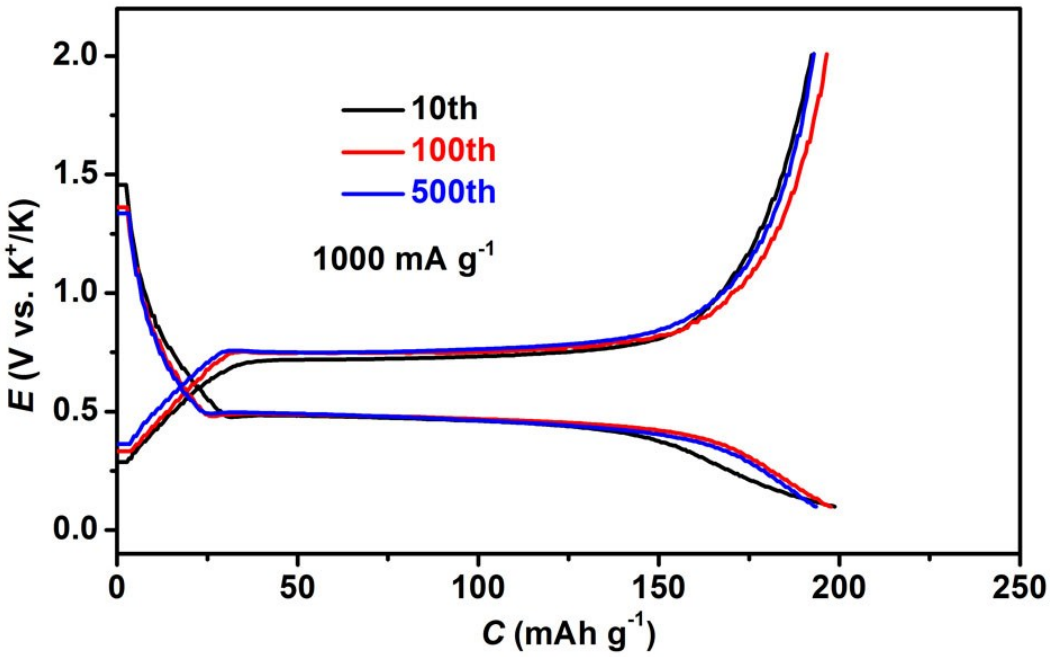

Fig. S6 Charge-discharge curves of the selected cycles at 1000 mA g^{-1}.

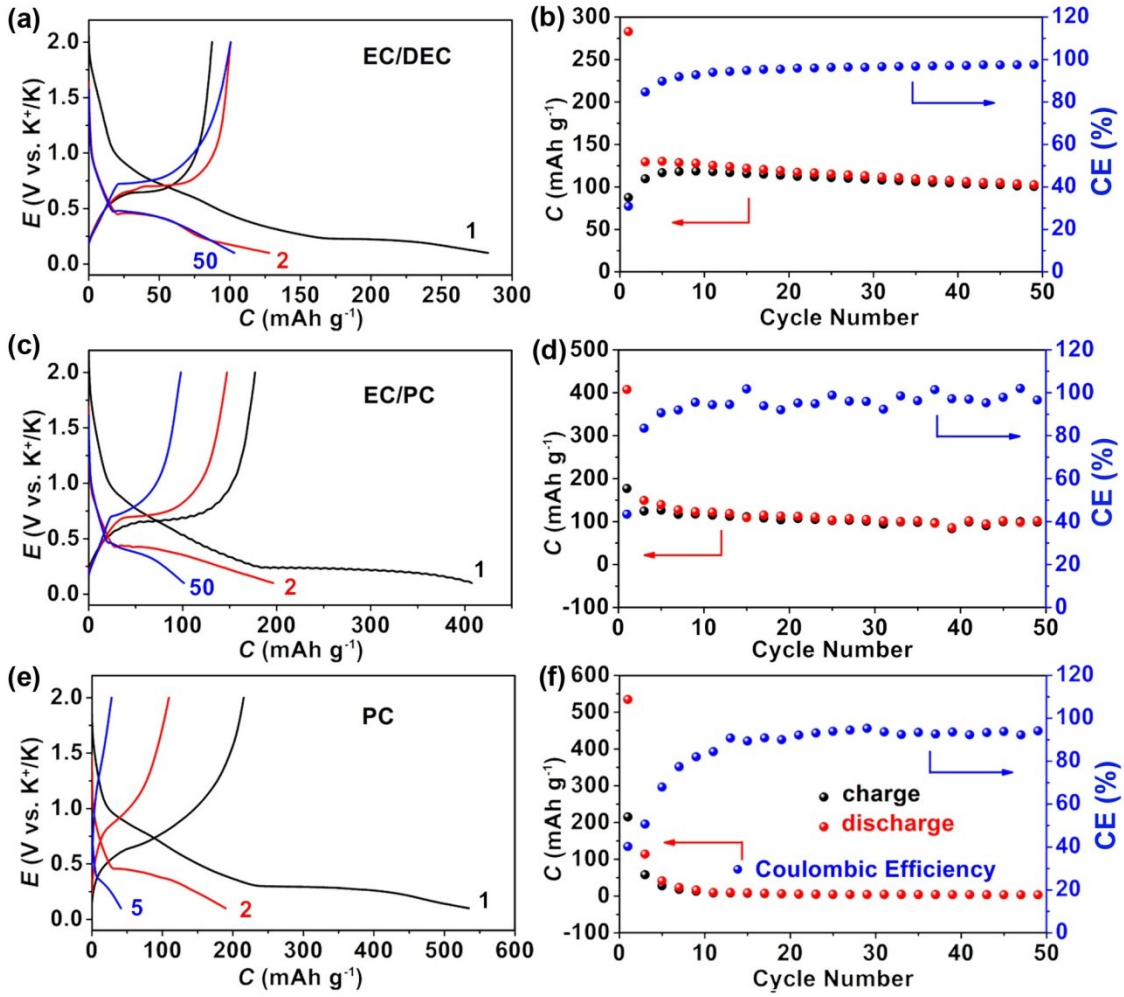

Fig. S7 Electrochemical performance of K_2TP at a current density of 50 mA g^{-1} in different electrolytes. (a, b) 0.8 M KPF_6/EC/DEC (1:1); (c, d) 1 M KPF_6/EC/PC (1:1); (e, f) 1 M KPF_6/PC.

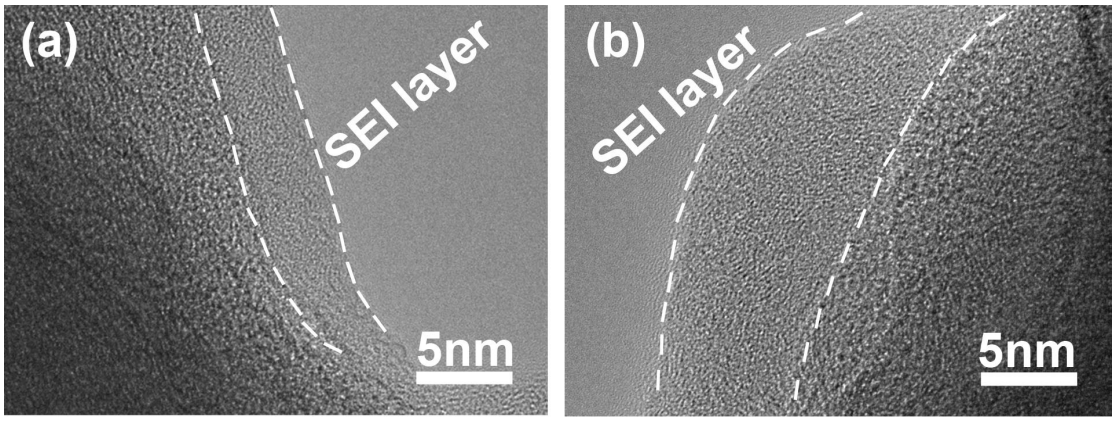

Fig. S8 High-resolution TEM images of the cycled electrodes in (a) DME- and (b) PC-based electrolyte.

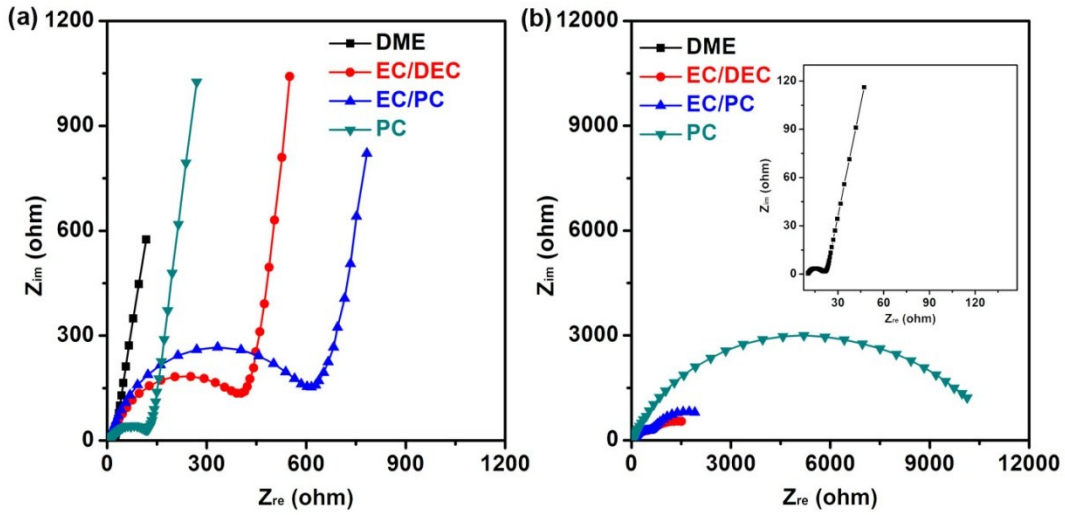

Fig. S9 EIS plots of K_2TP (a) at open-circuit voltage and (b) after 3 cycles.

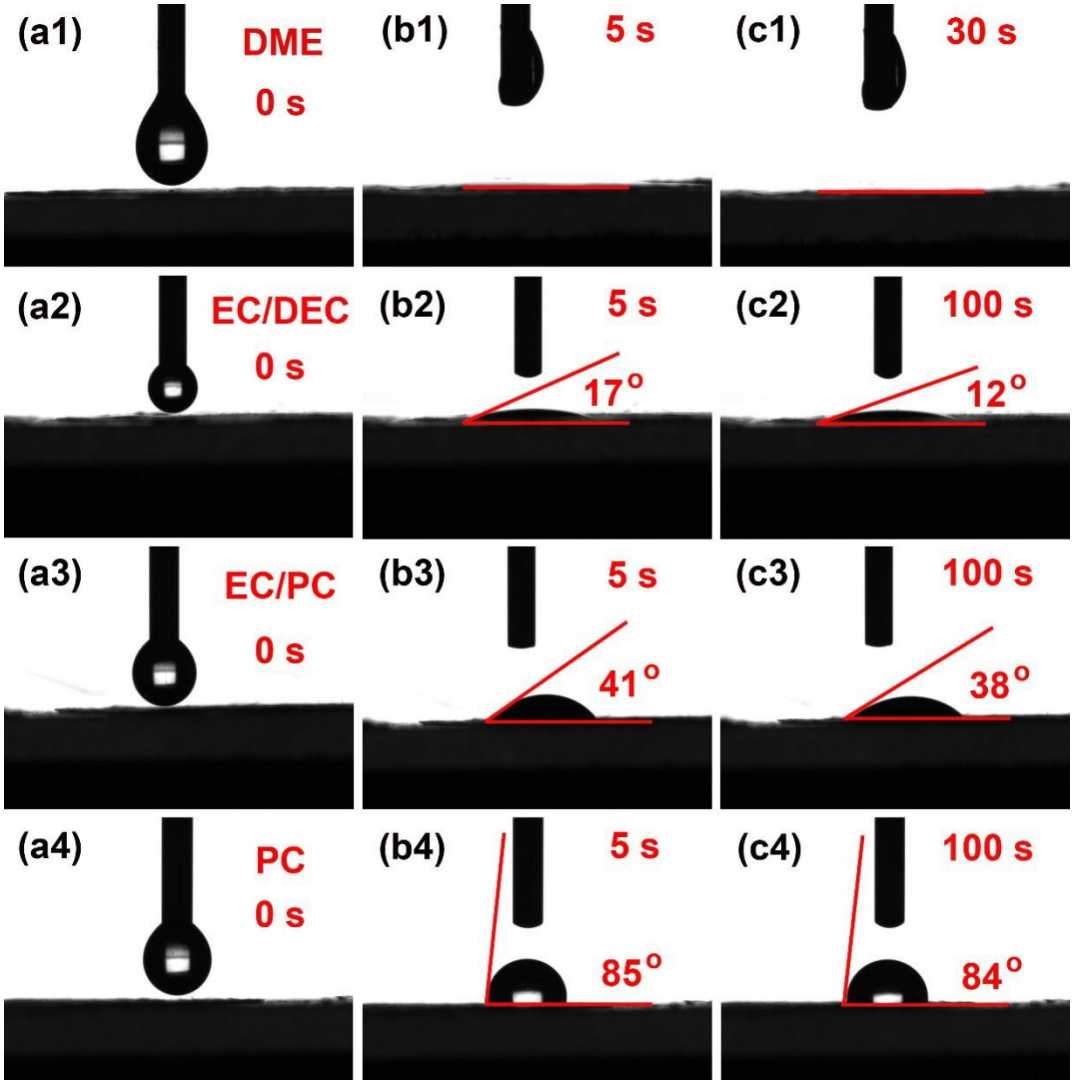

Fig. S10 Contact angles of the electrolytes on the K_2TP electrode.

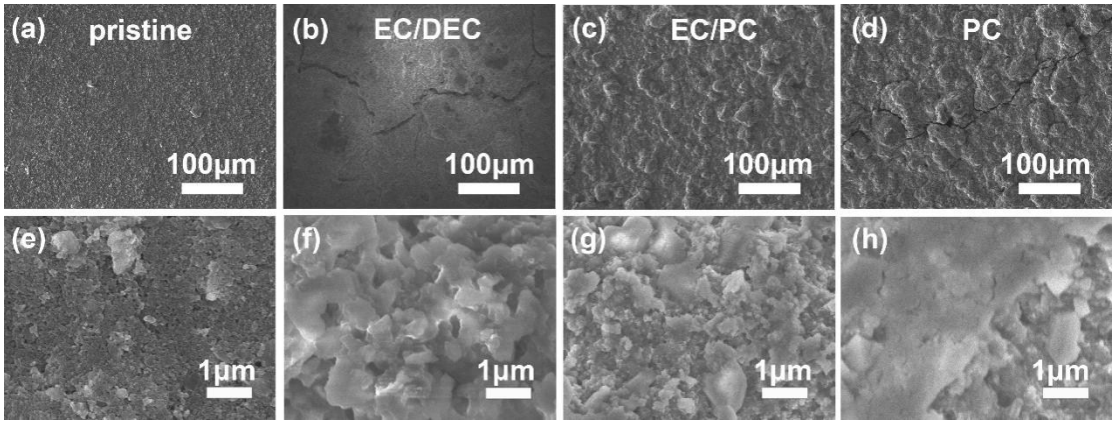

Fig. S11 SEM images of K_2TP electrodes (a, e) before cycling and after 50 cycles at 50 mA g^{-1} in (b, f) EC/DEC-based electrolyte, (c, g) EC/PC-based electrolyte, and (d, h) PC-based electrolyte.

Randles-Sevcik equation:

$$i_p = (2.69 \times 10^5) n^{3/2} A D_{K^+}^{1/2} C_{K^+} \nu^{1/2} \quad (1)$$

Where i_p is the peak current (A), n is the charge-transfer number, A is the contact area between electrode and electrolyte, D_{K^+} is the diffusion coefficient of K^+ ($cm^2\ s^{-1}$), C_{K^+} is the concentration of K^+ in the electrode material, ν is the scan rate ($V\ s^{-1}$).

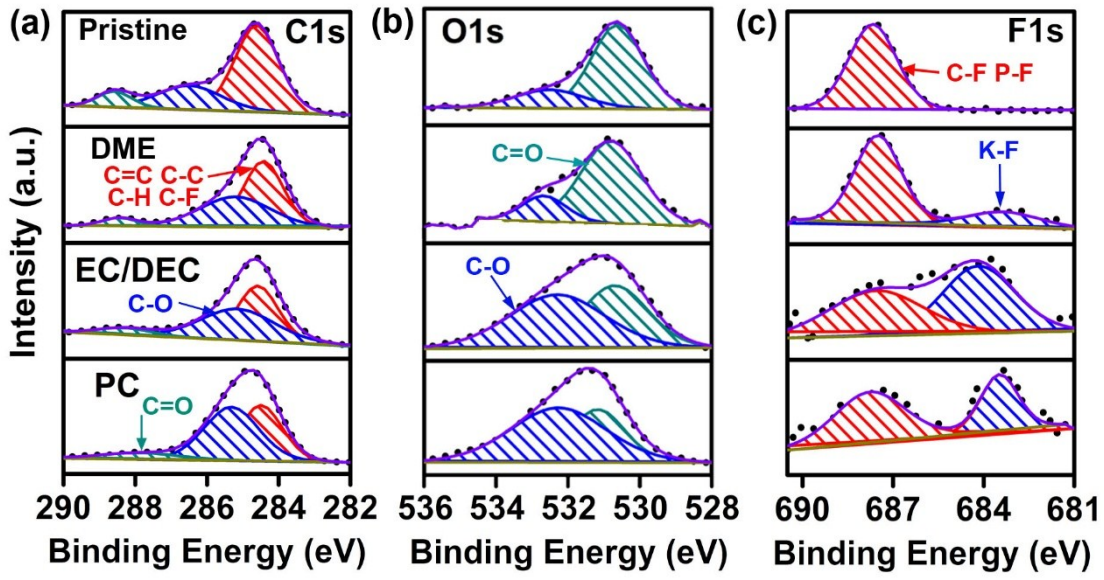

Fig. S12 Comparison of (a) C1s, (b) O1s, and (c) F1s spectra of the pristine electrode

and after the first cycle in the DME- and carbonate-based electrolytes.

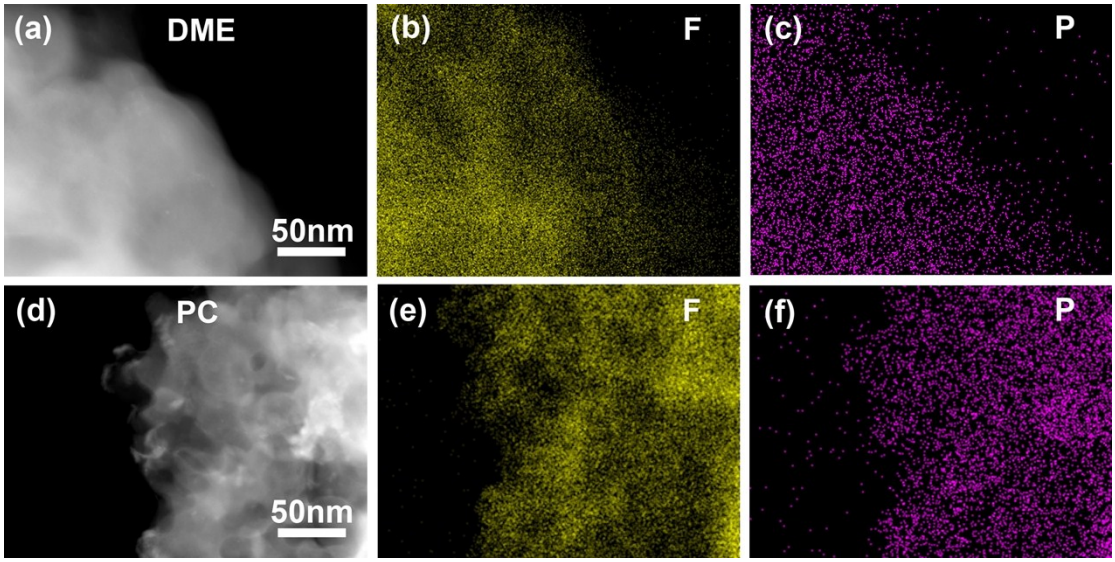

Fig. S13 Elemental mappings of the cycled electrodes in (a-c) DME- and (d-f) PC-based electrolyte.

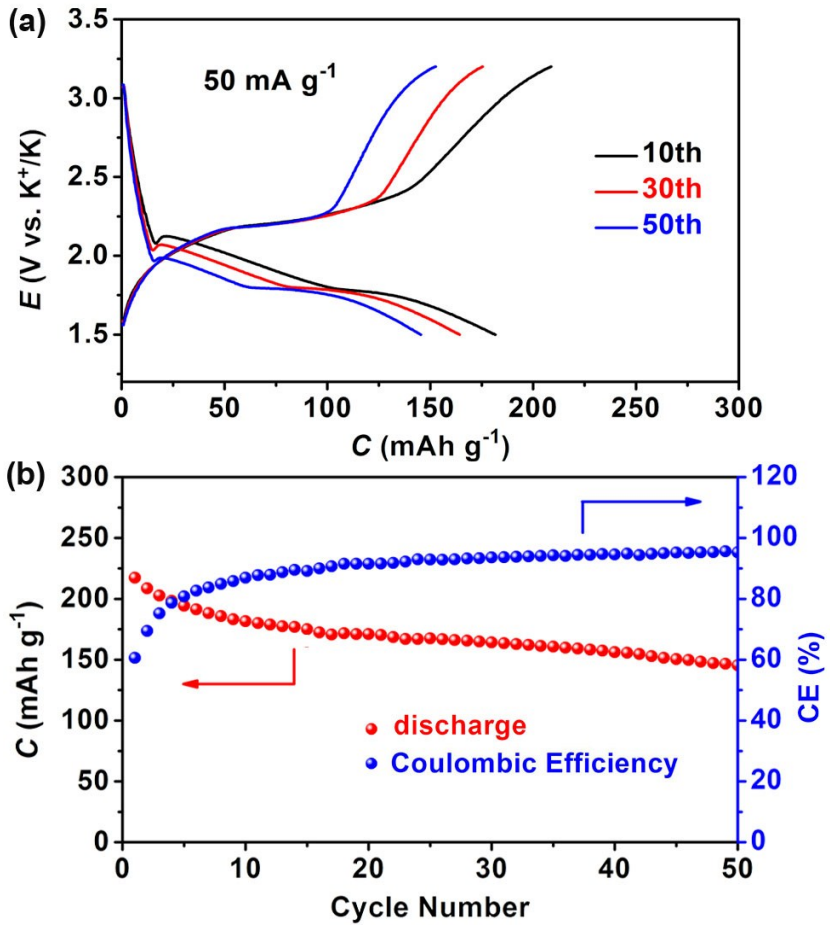

Fig. S14 (a) Charge-discharge curves of the selected cycles and (b) the cycling performance of $K_2(CO)_6/K_2TP$ full cell with excessive $K_2(CO)_6$ at 50 mA g^{-1}.

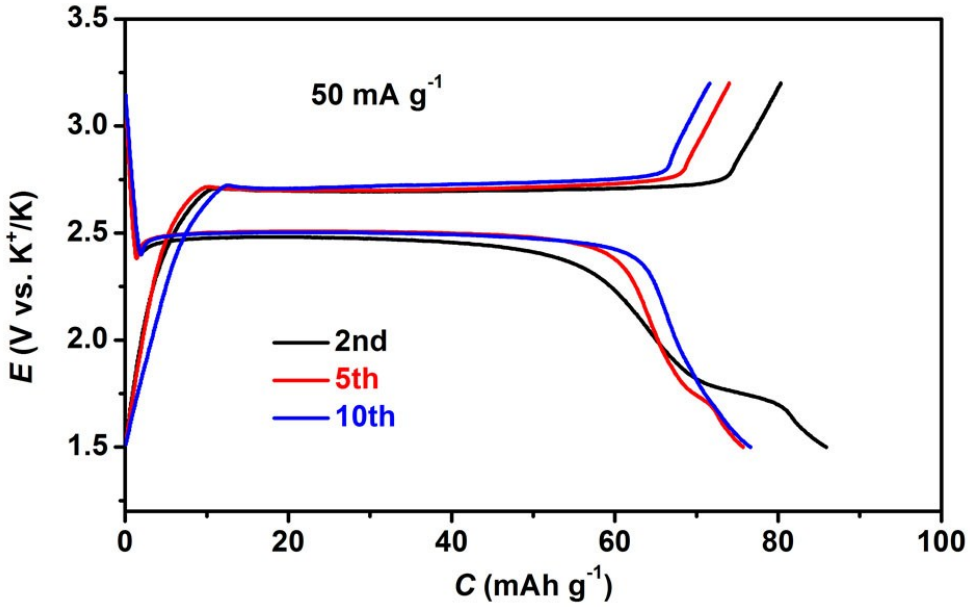

Fig. S15 Galvanostatic discharge/charge profiles of $K_2C_6O_6$ at 50 mA g^{-1}.

Table S2. Electrochemical performance comparison of some reported anode materials of KIBs.

Samples	Cyclability (capacity retention, compared with the 3rd cycle)	Rate performance	Ref.
K_2TP	229 mAh g^{-1} at 200 mA g^{-1}, 100 cycles (91.2%) 202 mAh g^{-1} at 500 mA g^{-1}, 100 cycles (91.8%) 194 mAh g^{-1} at 1000 mA g^{-1}, 500 cycles (94.6%)	261 mAh g^{-1} at 50 mA g^{-1} 249 mAh g^{-1} at 100 mA g^{-1}	This work
Hard Carbon	216 mAh g^{-1} at 27.9 mA g^{-1}, 100 cycles (83%)	240 mAh g^{-1} at 55.8 mA g^{-1} 229 mAh g^{-1} at 140 mA g^{-1} 136 mAh g^{-1} at 1395 mA g^{-1}	4
3,4,9,10-perylene–tetracarboxylicacid–dianhydride	160 mAh g^{-1} at 10 mA g^{-1}, 35 cycles (45.7%)		5
Sn-C	105 mAh g^{-1} at 25 mA g^{-1}, 30 cycles (63.6%)		9
Graphite	100 mAh g^{-1} at 140 mA g^{-1}, 50 cycles (50.8%)	234 mAh g^{-1} at 56 mA g^{-1} 172 mAh g^{-1} at 140 mA g^{-1} 80 mAh g^{-1} at 279 mA g^{-1}	11
$K_2Ti_8O_{17}$	110.7 mAh g^{-1} at 20 mA g^{-1}, 50 cycles (82%)	110 mAh g^{-1} at 40 mA g^{-1} 83 mAh g^{-1} at 100 mA g^{-1} 79 mAh g^{-1} at 150 mA g^{-1} 70 mAh g^{-1} at 200 mA g^{-1} 50 mAh g^{-1} at 400 mA g^{-1} 44.2 mAh g^{-1} at 500 mA g^{-1}	23
Carbon Nanofibers	80 mAh g^{-1} at 50 mA g^{-1}, 20 cycles (40%)		24
Graphite		150 mAh g^{-1} at 50 mA g^{-1} 90 mAh g^{-1} at 200 mA g^{-1}	25
RGO films	120 mAh g^{-1} at 10 mA g^{-1}, 100 cycles (80%)	200 mAh g^{-1} at 5 mA g^{-1} 98 mAh g^{-1} at 50 mA g^{-1} 60 mAh g^{-1} at 100 mA g^{-1}	25

Reference

[S1] M. J. Frisch, G. W. Trucks, H. B. Schlegel, G. E. Scuseria, M. A. Robb, J. R. Cheeseman, G. Scalmani, V. Barone, B. Mennucci, G. A. Petersson, H. Nakatsuji, M. Caricato, X. Li, H. P. Hratchian, A. F. Izmaylov, J. Bloino, G. Zheng, J. L. Sonnenberg, M. Hada, M. Ehara, K. Toyota, R. Fukuda, J. Hasegawa, M. Ishida, T. Nakajima, Y. Honda, O. Kitao, H. Nakai, T. Vreven, J. A. Montgomery, Jr., J. E. Peralta, F. Ogliaro, M. Bearpark, J. J. Heyd, E. Brothers, K. N. Kudin, V. N. Staroverov, R. Kobayashi, J. Normand, K. Raghavachari, A. Rendell, J. C. Burant, S. S. Iyengar, J. Tomasi, M. Cossi, N. Rega, J. M. Millam, M. Klene, J. E. Knox, J. B. Cross, V. Bakken, C. Adamo, J. Jaramillo, R. Gomperts, R. E. Stratmann, O. Yazyev, A. J. Austin, R. Cammi, C. Pomelli, J. W. Ochterski, R. L. Martin, K. Morokuma, V. G. Zakrzewski, G. A. Voth, P. Salvador, J. J. Dannenberg, S. Dapprich, A. D. Daniels, O. Farkas, J. B. Foresman, J. V. Ortiz, J. Cioslowski, D. J. Fox, Gaussian, Inc., Wallingford CT, **2009**.

[S2] A. D. Becke, *J. Chem. Phy.* **1988**, 88, 1053-1062.

[S3] C. Lee, W. Yang, R. G. Parr, *Phy. Rev. B* **1988**, 37, 785-789.

[S4] T. Lu, F. Chen, *J. Comput. Chem.* **2012**, *33*, 580-592.